

A Larger Extent for the Ophiuchus Stream

NELSON CALDWELL,¹ ANA BONACA,¹ ADRIAN M. PRICE-WHELAN,² BRANIMIR SESAR,³ AND MATTHEW G. WALKER⁴

¹*Center for Astrophysics | Harvard & Smithsonian, 60 Garden Street, Cambridge, MA 02138, USA*

²*Department of Astrophysical Sciences, Princeton University, Ivy Lane, Princeton, NJ 08544, USA*

³*Deutsche Börse AG, Mergenthalerallee 61, 65760 Eschborn, Germany*

⁴*McWilliams Center for Cosmology, Department of Physics, Carnegie Mellon University, 5000 Forbes Ave., Pittsburgh, PA 15213, USA*

ABSTRACT

We present new kinematic data for the Ophiuchus stellar stream. Spectra have been taken of member candidates at the MMT telescope using Hectospec, Hectochelle and Binospec, which provide more than 1800 new velocities. Combined with proper motion measurements of stars in the field by the Gaia - DR2 catalog, we have derived stream membership probabilities, resulting in the detection of more than 200 likely members. These data show the stream extends to more than three times the length shown in the discovery data. A spur to the main stream is also detected. The high resolution spectra allow us to resolve the stellar velocity dispersion, found to be $1.6 \pm 0.3 \text{ km s}^{-1}$.

1. INTRODUCTION

As discovered by Bernard et al. (2014), the Ophiuchus stream (OphStr) appeared to be a short and narrow stellar stream (2°5 long by 6′ wide), unlike most other known galactic stellar streams (Grillmair, & Carlin 2016). Bernard et al. (2014) used the then new PS1 catalog of stars for initial detection, and enhanced that by filtering out stars whose photometry did not fall in the area occupied by a metal-poor main sequence at heliocentric distances of 8 – 12 kpc. They calculated a luminosity for the entire stream to be $M_v = -3.0 \pm 0.5$, similar to that found for the lowest mass galactic globular clusters. Sesar et al. (2015) followed up the imaging work with a spectroscopic project that showed the stream to have a high heliocentric radial velocity of 290 km s^{-1} , nearly 300 km s^{-1} different from the mean of the majority of stars at that position. This large offset mitigates the often difficult problem of distinguishing stream members from nonmembers. Using MMT/Hectochelle and Keck/Deimos, fourteen radial velocity members were found: six blue horizontal branch stars (BHB), two main-sequence turnoff stars, one subgiant (SG), and five red giants (RGB), four of which had spectra with high enough signal-to-noise to allow a determination of atmospheric parameters. An analysis showed those stars to be alpha enhanced, and of low metallicity, indicating

that the progenitor of the stream was likely a globular cluster. The stream was then thought to extend from galactic longitude $l = 3^\circ 8'$ to $5^\circ 8'$, for a physical projected length of 300 pc at a mean heliocentric distance of 8 kpc and a variation of about 1.5 kpc over that angle, with the western end being more distant. The galactic latitude of the stream in the Sesar et al. paper extended over the range of $b = +30.5$ to 32 ; the paper used the measured velocity dispersion to estimate the initial mass to be $2 \times 10^4 M_\odot$.

The OphStr appeared very different from other known streams which span many tens of degrees on the sky, thus leading Sesar et al. (2015) to postulate it was created within a 1 Gyr short time period or required special circumstances. Sesar et al. (2016) suggested that bar-induced fanning would have the effect of lowering the surface density at large distances along the stream, making the detection more difficult and thus causing the stream to appear shorter than it actually is.

Further spectral observations on 43 stars selected to have BHB star colors initially indicated this might be the case. Six of those stars had radial velocities indicating membership (we show below that one is not a member based on proper motions). Several of these were positioned at large angles from the main stream, beyond galactic longitude 6° where the discovery image shows no stream, resulting in a revised deprojected length estimate of 2 to 3 kpc, depending on which stars were believed to be members. Price-Whelan et al. (2016) and Hattori et al. (2016) investigated possible scenarios where a rotating galactic bar can create a shortened

stream and a high velocity dispersion for nearby stars. Lane et al. (2019) used the published radial velocities and proper motions from the recent release of the Gaia-DR2 catalog (GDR2, Gaia Collaboration et al. 2018) to further simulate the orbit, finding that the stream is likely only on its second pericenter passage. But there is a clear lack of radial velocity data extensive enough to allow models to be verified, and thus a third, larger scale observational project is warranted to further explore the dimensions of the stream and the dynamical history of it. This paper describes that spectroscopic project, involving three different spectrographs on the MMT, and complemented with the GDR2 data. The spectroscopic data continues to be heterogeneous. Our paper describes the observations in the time order they were taken.

2. NEW HECTOSPEC OBSERVATIONS

2.1. Target Selection

Although the stream is narrow in the discovery image (6' FWHM), it is prudent to probe a wide area to avoid missing the true distribution. Hectospec/Hectochelle (Fabricant et al. 2005) with its 1° field is ideal for this, and indeed a few giant stars were observed in one field for Sesar et al. (2015), centered on the densest part of the stream. The limiting magnitude of the stars observed with Hectochelle in 2014 for Sesar et al. (2015) was $i=18.8$ ($g=19.2$), at the top of the turnoff of the main sequence (MSTO) of the stream (see Fig 1). Most of the member stars successfully observed were on the giant branch about 1.5 mag below the level of the horizontal branch and 1.0 mag brighter than the MSTO. For a subsequent project, we wanted to observe fainter MSTO targets, which are of course far more numerous than BHB, RGB or SG stars, but would be out of reach for the high dispersion Hectochelle spectrograph (resolution=32000), and thus it was thought best to use a lower resolution option for the more extensive member search, and employ Hectospec, which gave a resolution of 2400.

A new observing catalog was made, using the PS1 gri data (Kaiser et al. 2010), with a data filter that selected putative MS turnoff stars. The original selection used PS1 data corrected for reddening with the Schlegel et al. (1998) dust map (the mean reddening for the stream is $E(B-V)=0.185$). Nine 1° fields were identified to sample along the model orbit of Sesar et al. (2015), where stars were included with $(g-i)_0$ color within 0.1 mag of the best-fit OphStr isochrone (from PARSEC, corrected for extinction, Bressan et al. 2012), bluer than $(g-i)_0 = 0.3$ mag, and uncorrected g brighter than $g = 21$ mag. Sesar et al. (2015) had detected a distance

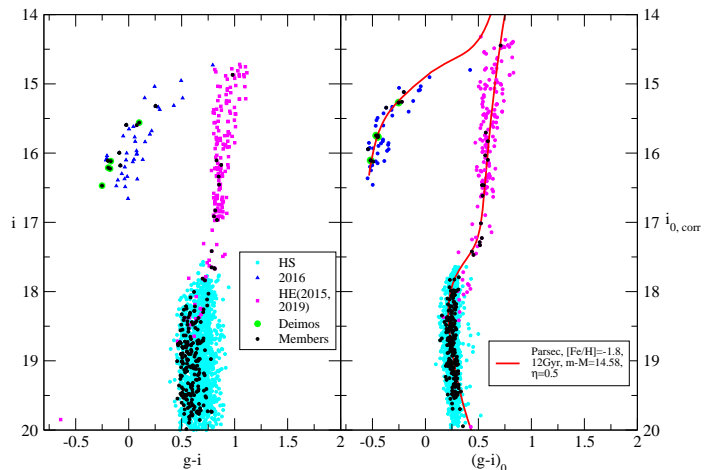


Figure 1. CMD of input stars. Left panel shows the uncorrected PS1 photometry while that on the right has been corrected for local reddening, and the distance modulus gradient derived in Sesar et al. (2015). Three previous sets of observed stars are indicated by different colored symbols, with black filled circles representing radial velocity members from all sources, mostly those reported here. Magenta circles were observed by Hectochelle (in two epochs), while green represents Deimos observations, reported in Sesar et al. (2015). Blue circles are observations of BHB stars reported in Sesar et al. (2016). Cyan points are the stars selected, and observed as part of the Hectospec program reported here. A PARSEC isochrone (Bressan et al. 2012) is also shown which has parameters: age=12 Gyr, $[Fe/H] = -2.0$, mass loss parameter $\eta = 0.5$, and $m-M=14.58$, the mean distance modulus derived in Sesar et al. (2015). The star selection for spectroscopic observations was based on the right panel, using MSTO stars near the isochrone as described in the text. A few stars appear redward of the main group because we changed the source of the reddening map between making the catalog and writing this paper, and some photometric values changed in the source catalog in that period as well.

modulus gradient ($m-M = 14.58 - 0.2(l - 5)$, where l is the galactic longitude), and that was also employed in the star selection (the value is called $i_{0,corr}$). The reddening values vary by as much as 0.2 mag in $E(B-V)$, so the uncorrected colors show a wider distribution than the corrected colors. After the observations were made, we began to use the updated Schlafly et al. (2014) map, which has a few individual star differences, and thus some stars appear outside of the original color-mag selection box in Fig 1. The net result is that selected stars had dereddened i between 17 and 20 mag, and $(g-i)_0$ colors between 0.15 and 0.3 mag.

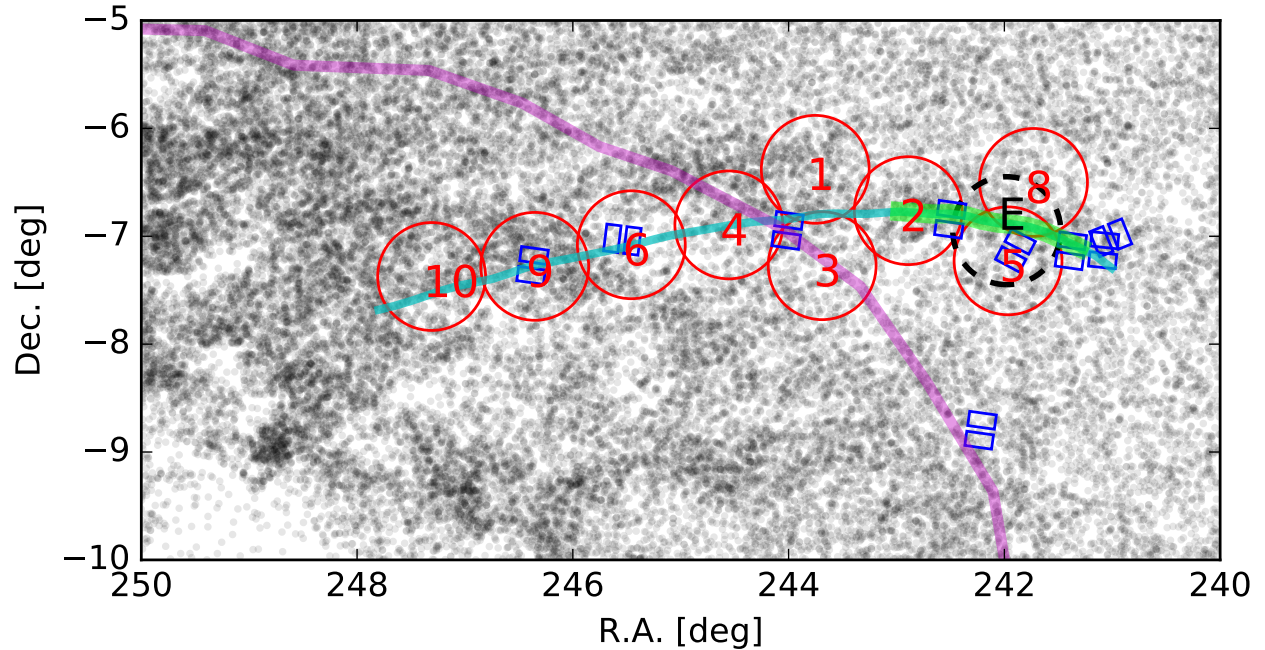


Figure 2. Distribution of stars in the Ophiuchus Stream field selected to be MSTO stars as shown in Fig 1 (the cyan dots in that figure). The nine Hectospec 1° fields are shown in red, along with the approximate distribution of the stream initially published by Bernard et al. (2014), shown as a thick solid green line. The positions of the circles outside of the initial stream were meant to follow the expected distribution determined by the orbit model of Sesar et al. (2015), shown as a thin cyan line. (Hectospec field number 7 was not observed.) The nine Binospec fields discussed in Section 3 are shown as pairs of blue rectangles. The 2019 HectoChelle field is shown as a black dashed circle, with an “E”. The ζ Oph H II region is strong to the east (left) of the magenta line, and thus affects all the Hectospec fields except 1, 2, 5 and 8, with the emission getting stronger in the east direction.

Fig. 1 shows the target selection in those nine fields, along with previously known members, and members found here. Note that the members fall within the color spread of the candidates, thus systematics have been minimized. Fig. 2 shows the on-sky distribution of those stars and the surrounding ones with the same selection criteria. Below, we will refine the CMD selection based on radial velocity membership for a second round of new

observations with the Binospec instrument. The actual observing conditions varied among the different fields for the Hectospec data, so the depths explored are quite different.

The MSTO stars are hot enough so that Balmer series lines are prominent, which will thus provide the dominant signal for radial velocity measurements. Upon examining the raw data, we noticed a number of the

fields showed Balmer emission, which we realized after the observations were already taken was due to the eastern part of the stream overlapping on the sky with the large ζ Oph H II region (Haffner et al. 2003). This complicated the data reduction, as multifiber spectroscopy typically does not use local sky measurements. The fact that the dominant feature in our stars is Balmer absorption further meant that for some spectra the emission contamination precluded the measurement of a believable stellar velocity.

2.2. Details of Hectospec Observations

A total of 9 separate Hectospec fields were observed in 2016 using the MMT and Hectospec instrument with the 600gpm grating, which gave spectra in the range of $\lambda\lambda 4030 - 6500\text{\AA}$, with a resolution of 2.3\AA . An important caveat in this data set is the variable conditions for the different fields, making the success rates of obtaining useful spectra (which give dependable radial velocities) vary by a large factor among the fields. For six of the fields we had an average success rate of nearly 90% but for the other three we obtained an average less than 50%. Sixty two stars were observed in two separate configurations. Table 1 gives the details of the fields observed. Data were processed using the method outlined in Caldwell et al. (2009) with the exception of how the sky subtraction was done. Sky fibers near the targets were chosen rather than a sum of all sky fibers, due to the variable strength of the Balmer emission from the H II region. This method still left a few stars poorly sky subtracted, resulting in deep features that could be picked up by a velocity finding program (the velocity of the H II region is about -11 km s^{-1} , similar to the mean of the non-stream stars) and thus resulting in faulty radial velocities. These spectra were noted individually and removed from the catalog. More than 1700 stars were observed with Hectospec.

Heliocentric radial velocities were found using *xcsao* (Kurtz & Mink 1998), in the spectral range of $\lambda\lambda 4200 - 5300\text{\AA}$; this range gave the cleanest cross-correlation functions and hence the lowest formal errors. Templates used were model atmosphere spectra supplied by C. Johnson, all at $T_{eff} = 6000$ and $\log g = 4$, but four metallicities ($[\text{Fe}/\text{H}] = -2, -1.5, -1.0, -0.5$ and 0). The general features of these templates match those of the expected spectra of the targeted MSTO stars (the predominant lines are the Balmer series, though Mgb and the stronger Fe lines are also present).

For many of the repeated stars, one observation had S/N too low to obtain a significant velocity; just five repeated stars had small enough errors for analysis. For those pairs we determine an RMS difference of 10

km s^{-1} , meaning the true RMS is $10/\sqrt{2} = 7 \text{ km s}^{-1}$, somewhat smaller than the mean formal velocity uncertainty for the stars of 13 km s^{-1} . Four stars were in common with the earlier Hectochelle data, where the formal velocity uncertainties are an order of magnitude smaller. We find the RMS difference between these to be 10 km s^{-1} , with the formal RMS being 20 km s^{-1} . Again, the true RMS is likely to be smaller than the formal errors reported in the Table 2 (below).

It would be ideal to do a full fit to these spectra to derive stellar properties, but we postpone that till a later paper, so that we can present the main result in a timely manner. The high radial velocity of OphStr made it unlikely we would have included too many nonmembers by simply making an initial membership selection using only radial velocity.

2.3. The Stream in Radial Velocity Space

We were fortunate that the OphStr has a radial velocity of nearly 300 km s^{-1} different from the mean of the field stars present. This allows us to make a fairly clean initial assessment of membership based on radial velocity alone, which we will then use to refine the CMD selection and include a proper motion and position selection as well.

We present the histogram of all radial velocities with significant detections in Fig 3. Included here are the new Hectospec data, the radial velocities from Sesar et al. (2015) and Sesar et al. (2016), as well as the other new data to be reported in sections below. The mean velocity is around 290 km s^{-1} , which we will refine below. Stars within $5'$ of the Sesar et al. (2015) orbit model (in red) show a stronger velocity contrast than the sample as a whole. The bottom panel, plotting radial velocities as a function of RA, also clearly shows the separation of the stream from the background. Table 2 contains the spectroscopic data. Items listed are those for which we have spectra of any quality. If the derived radial velocity was considered flawed, the velocity entry is blank, but the correlation coefficient R is listed (in broad terms, R values greater than 4 means that the derived radial velocity can be trusted.) Items where no GDR2 proper motions are available are still listed if a spectrum was taken, even if it was poor. The table is organized such that stars with membership probabilities greater than zero are listed first, in order of RA. The second group has stars with probabilities equal to zero, or for which we have no determination.

2.3.1. Reddening

We used the Schlafly et al. (2014) map to correct the PS1 photometry, noting that the kernel size for this map is about the width of the stream, which could lead to

Table 1. Observation Log

field	Inst ^a	Date	RA	Dec	Exposures	Seeing ^b	% Good
			J2000		(sec)		
1	H	2016.0311	16:15:00.7	-06:22:46.9	3 × 1800	1.0	68
2	H	2016.0313	16:11:33.9	-06:45:45.9	3 × 1500	0.7	94
3	H	2016.0314	16:14:45.3	-07:16:22.9	4 × 1800	0.9	98
4	H	2016.0316	16:18:12.9	-06:53:40.9	3 × 1800	0.7	93
5	H	2016.0417	16:07:51.7	-07:13:40.6	3 × 1800	2.2	31
6	H	2016.0417	16:21:49.8	-07:04:44.2	3 × 2100	2.2	47
8	H	2016.0418	16:06:55.1	-06:30:03.6	3 × 2100	1.7	83
9	H	2016.0419	16:25:24.8	-07:16:44.4	4 × 1800	1.5	44
10	H	2016.0317	16:29:14.1	-07:22:22.9	3 × 1800	0.8	91
11	B	2018.0410	16:07:35.4	-07:07:52.5	3 × 600		81
12	B	2018.0410	16:04:03.5	-07:00:53.1	3 × 600		82
13	B	2018.0411	16:08:53.0	-08:47:53.2	3 × 600		98
14	B	2018.0411	16:22:09.8	-07:01:52.1	3 × 600		91
15	B	2018.0604	16:05:32.1	-07:08:04.9	3 × 1200		88
16	B	2018.0605	16:04:19.2	-07:07:47.5	3 × 1200		79
17	B	2018.0608	16:10:00.4	-06:50:34.7	3 × 1200		95
18	B	2018.0612	16:16:02.3	-06:57:45.9	3 × 1200		72
19	B	2018.0613	16:25:29.7	-07:16:13.3	3 × 1200		89
20	E	2019.0622	16:07:54.8	-06:56:54.0	6 × 2600	1.1	43

^aH=Hectospec, B=Binospec, E=Hectochele

^bin arcsecs. Seeing values were not recorded during the Binospec runs.

some circular problems in determining the reddenings. The mean reddening over the stream is 0.185, with a range from 0.408 to 0.139 (the median value is similar to the mean).

2.3.2. Distance confirmation

From their 14 member stars, Sesar et al. (2015) derived a distance modulus and gradient in the modulus, specifically $m-M = 14.58 - 0.2(l - 5)$, where l is the galactic longitude (thus giving a distance of 8.2 kpc at $l = 5$). We confirmed this in general for our new sample of MSTO stars we have observed, without rederiving a new value with the rigor that Sesar et al. (2015) employed. Fig. 4 shows the CMD of stars with membership probability $P_{\text{mem}} > 0.9$ (see Sect. 6) in two widely separated parts of the stream: the western part, from $l = 3^{\circ}.7$ to $5^{\circ}.4$ (75 member stars), and the eastern part,

from $l = 5^{\circ}.4$ to $7^{\circ}.0$ (55 stars). A simple comparison of the PS1 ($g - i$) CMD of the similar metallicity globular cluster NGC 5466 with that of the OphStr members (using dereddened photometry) reveals that the stated distance modulus and gradient is satisfactory for the

MSTO stars and the HB stars to within 0.15 mag, but is not as good for the member RGB stars (11 in total, including the ones found in the Hectochele observations), with the stars being 0.05 mag bluer in the ($g - i$) color than expected from the relative position of the MSTO stars, which could be due to a difference in stellar populations between NGC 5466 and the stream.

3. BINOSPEC DATA

This instrument is a new low-resolution, multi-slit spectrograph on the MMT, which features two $8 \times 15'$ fields (Fabricant et al. 2019). Although the field is smaller than Hectospec, the extra depth afforded made it attractive, and some telescope time became available during the first months of operation. We employed the 1000 gpm grating which gives spectral resolution of 1.5 \AA over a range of 1500 \AA . We centered the spectra at 5200 \AA which allowed the inclusion of the $H\beta$ line as well as the Mg b lines. Slit widths were $1''$, and lengths were typically more than $20''$ long. The OphStr Binospec observation information is also contained in Table 1.

Table 2. Spectroscopic Observations. This is a stub; full table to appear in the journal.

S^a	RA	DEC	b	i	$(g-i)_0^c$	i_0	V	R	μ_α^*	μ_δ	π^d	D^E	P^{mem}
							km s $^{-1}$		mas yr $^{-1}$	mas yr $^{-1}$	mas	arcmin	
B	240.97155	-7.18619	19.515±0.027	19.010±0.021	0.244±0.034	18.715	284.1±20.4	5.6	-3.948±0.934	-4.909±0.490	0.308±0.424	9.7	0.93
B	240.98628	-7.02181	19.462±0.015	19.005±0.035	0.195±0.038	18.710	277.9±50.3	3.0	-3.562±0.979	-3.148±0.477	0.112±0.444	0.2	0.98
B	240.98870	-7.18613	19.885±0.042	19.383±0.014	0.239±0.044	19.087	272.0±19.7	5.2	-3.047±1.786	-3.562±0.883	-0.580±0.724	9.9	0.97
B	240.99936	-6.89888	20.006±0.054	19.546±0.041	0.204±0.068	19.258	206.9±28.8	3.1	-5.764±1.248	-4.237±0.659	-0.023±0.677	6.9	0.70
B	241.04199	-7.18313	19.337±0.029	18.792±0.025	0.281±0.038	18.494	260.4±17.1	7.0	-4.118±0.922	-5.120±0.423	-0.216±0.382	10.4	0.98
B,B	241.09955	-7.08248	19.402±0.027	18.892±0.023	0.243±0.035	18.591	282.0±15.5	5.3	-3.974±0.858	-4.302±0.414	-0.195±0.380	5.1	0.99
B	241.10806	-7.14182	21.102±0.088	20.480±0.099	0.354±0.132	20.178	264.0±31.8	3.3	-0.052±4.092	-4.078±1.533	-0.418±1.443	8.7	0.91
B,B	241.11475	-7.17195	20.105±0.038	19.605±0.051	0.234±0.064	19.305	286.5±22.0	2.8	-4.217±1.659	-4.363±0.790	0.307±0.785	10.5	0.99
B	241.12453	-7.16020	20.464±0.054	19.895±0.043	0.302±0.069	19.594	353.5±24.3	3.5	-8.540±1.860	-4.556±0.847	1.073±0.861	10.0	0.89
B	241.15885	-7.08421	20.049±0.087	19.503±0.044	0.287±0.097	19.204	337.6±23.6	3.7	-4.732±1.559	-4.689±0.671	0.450±0.702	5.8	0.99
B	241.18693	-7.09031	20.040±0.077	19.481±0.034	0.293±0.084	19.181	307.8±25.7	3.5	-6.119±1.481	-4.754±0.630	0.887±0.741	6.5	0.99
B	241.25540	-7.11738	20.229±0.046	19.701±0.076	0.265±0.089	19.403	291.5±20.7	5.0	-0.449±1.558	-5.054±0.712	-0.704±0.868	8.8	0.93
B	241.26994	-7.09292	19.700±0.029	19.211±0.038	0.227±0.048	18.914	308.6±22.5	5.5	-5.920±1.036	-4.117±0.492	0.679±0.364	7.5	0.99
B	241.28172	-7.08352	19.034±0.033	18.479±0.016	0.293±0.037	18.183	276.4±15.8	7.4	-4.146±0.634	-4.601±0.306	0.014±0.346	7.1	0.99
B	241.30041	-7.09073	19.995±0.039	19.497±0.033	0.237±0.051	19.201	269.1±17.0	6.6	-3.246±1.286	-4.573±0.717	-0.271±0.567	7.7	0.98
B	241.30960	-7.02269	19.286±0.036	18.740±0.027	0.282±0.045	18.441	311.4±18.0	6.5	-6.173±0.802	-1.888±0.363	0.134±0.327	3.8	0.55
B	241.31232	-7.21352	19.393±0.032	18.899±0.016	0.230±0.036	18.602	301.4±15.9	6.9	-3.796±0.789	-4.576±0.385	0.484±0.519	15.1	0.99
B	241.33822	-7.06355	19.238±0.017	18.746±0.023	0.231±0.029	18.450	256.0±21.4	6.0	-4.761±0.746	-4.041±0.355	0.053±0.323	6.5	0.98
B	241.33883	-7.10237	19.058±0.036	18.550±0.031	0.246±0.048	18.254	263.3±14.8	7.2	-4.824±0.626	-4.591±0.305	-0.036±0.282	8.8	0.99
B	241.41009	-7.08610	19.925±0.071	19.410±0.029	0.253±0.077	19.115	244.0±14.4	8.4	-4.043±1.332	-5.079±0.739	0.470±0.577	7.9	0.95
B	241.39887	-7.02366	19.832±0.073	19.356±0.046	0.209±0.086	19.056	270.7±21.6	5.2	-3.421±1.463	-4.219±0.645	-0.995±0.546	4.7	0.99
H	241.40146	-6.36448	19.730±0.054	19.112±0.042	0.277±0.068	18.727	313.9±28.4	5.9	-4.459±0.931	-3.615±0.542	-0.195±0.443	34.4	0.97
B	241.41009	-7.05488	20.419±0.061	19.844±0.059	0.310±0.085	19.544	331.8±26.9	4.3	-5.694±2.218	-3.673±0.963	-0.606±0.815	6.6	0.98
B	241.41503	-7.07013	20.042±0.043	19.475±0.086	0.301±0.096	19.175	263.4±12.8	7.5	-5.383±1.536	-5.267±0.714	1.295±0.631	7.6	0.98
B	241.43110	-7.06141	19.964±0.056	19.475±0.049	0.222±0.074	19.174	274.3±23.4	4.7	-6.056±1.488	-3.814±0.744	0.447±0.608	7.2	0.98
B	241.44318	-7.01940	20.047±0.073	19.531±0.032	0.247±0.080	19.229	280.2±16.5	7.4	-4.491±1.518	-4.615±0.835	0.988±0.644	4.9	0.99
B	241.44472	-6.99315	19.964±0.035	19.459±0.051	0.237±0.062	19.155	275.7±21.9	5.0	-5.604±1.142	-4.136±0.611	-0.526±0.525	3.3	0.99
B	241.44686	-7.02205	20.161±0.076	19.641±0.091	0.252±0.119	19.338	220.6±22.3	4.8	-3.877±1.440	-4.332±0.768	-0.201±0.714	5.0	0.85
B	241.47695	-6.98119	20.182±0.074	19.618±0.061	0.295±0.096	19.313	300.1±21.7	4.2	-3.504±1.304	-4.792±0.924	-0.561±0.706	2.9	0.99
D	241.49994	-7.03410	16.018±0.021	16.211±0.013	-0.465±0.025	15.903	285.3±1.9	5.0	-4.620±0.197	-4.382±0.120	0.040±0.096	6.2	0.99

^a Source. A=Sesar et al. (2016), E=Hectochelle(Sesar et al. 2015), D=Deimos (Sesar et al. 2015), H=Hectospec, B=Binospec, F=Hectochelle 2019 (the latter three reported here)

^b Photometry from PSI

^c Dereddened using the maps of Schlafly et al. (2014)

^d Parallaxes are as reported in GDR2; we do not add in the +0.05 mas correction as discussed in the text.

^e Angular distance to stream fiducial

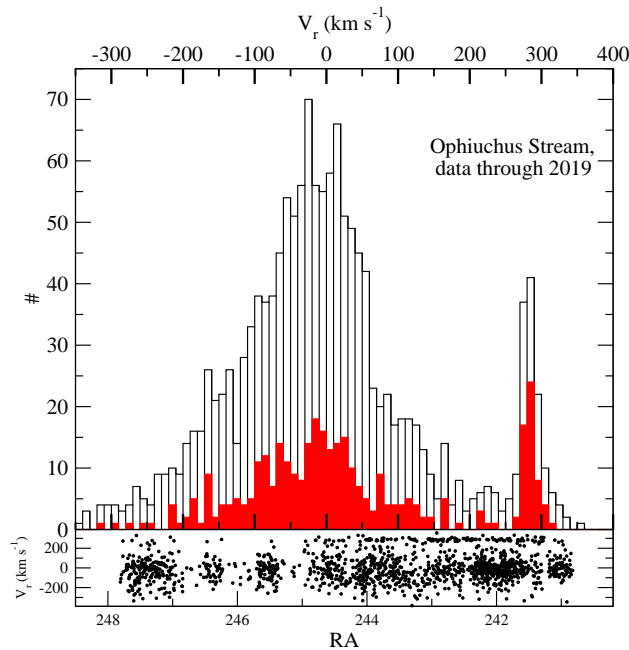


Figure 3. Top: The histogram of well-determined radial velocities from Hectospec, the two previous papers (Sesar et al. 2015, 2016), the Binospec data, and the Hectochelle data from this paper, binned into 10 km s^{-1} bins. The stream stands out clearly at a velocity near $+300 \text{ km s}^{-1}$. The red histogram shows just stars within $5'$ of the orbit shown in Fig. 2. Bottom: the distribution of radial velocities with RA, also showing the stream separation in velocity.

We selected fields to overlap some of the Hecto fields, particularly where the Hecto data was compromised by bad observing conditions, but also to explore the ends of the apparent stream, as well as a field well off of the visual stream as a control, as shown in Fig. 2.

Stars on the main sequence as described above were selected (they generally occupy the same part of the CMD as the Hectospec observations shown in Fig 1), as well as some lower RGB stars (none of the latter turned out to be members). The catalog had fainter stars than the Hectospec sample (down to $i = 21$), but only 20% of the spectra for stars fainter than $i = 21$ provided good velocities (furthermore, only a handful of stars fainter than $i = 20.4$ have GDR2 measurements).

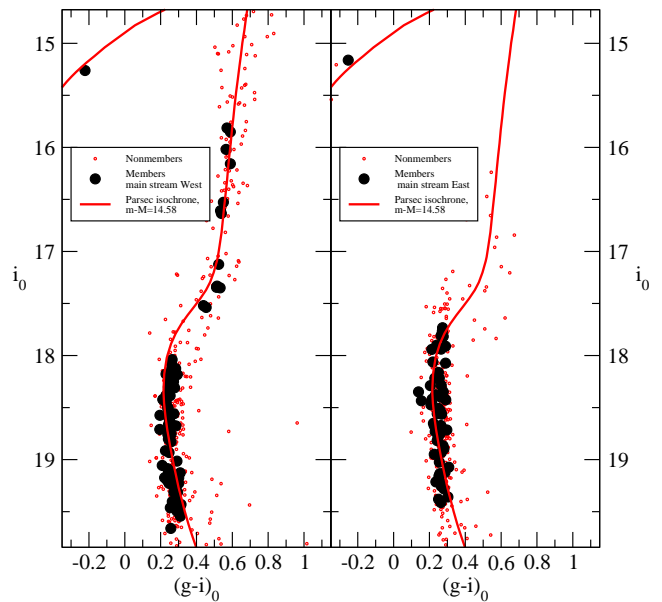


Figure 4. CMD of high probability member stars ($P_{\text{mem}} > 0.9$), divided into two parts at opposite ends of the densest part of the stream, to show the evidence for a distance difference for those parts. Left: the western part, from $l = 3^{\circ}.7$ to $5^{\circ}.4$ (75 member stars). Right: the eastern part, from $l = 5^{\circ}.4$ to $7^{\circ}.0$ (55 stars). The Parsec isochrone uses the same distance modulus in both panels. Note the MS turnoff occurs at a brighter magnitude for the eastern part of the stream. These stars are within $10'$ perpendicular to the long axis of the stream. Red circles indicate stars observed but which had radial velocities precluding membership.

Two separate runs were obtained in 2018, with the first extending to $i = 21$, while the second only to $i = 20$. The statistics reported in Table 1 limit the first set to $i = 20$ for comparison. Heliocentric radial velocities were found as above for the Hectospec data, using the same templates. More than 800 stars were observed, making for a total of 2600 unique objects observed in all the various projects to date to obtain spectra in OphStr. Six stars were observed twice, giving an RMS error for measurement of 10 km s^{-1} .

There were 26 stars observed both with Hectospec and Binospec; 23 of those have good velocities for both measurements. The mean velocity difference of those was $+1.1 \text{ km s}^{-1}$ (Hectospec – Binospec), with an RMS of the differences of 16 km s^{-1} , or 11 km s^{-1} per star in the mean for each sample if they have the same error distribution. The mean formal errors provided by xcsao for those Binospec stars is 15 km s^{-1} , so the formal errors are somewhat larger than the true errors, but we will assume the formal errors are accurate for the analyses below.

4. USING GAIA DR2 TO REFINE A CANDIDATE LIST

We next incorporated the new Gaia DR2 proper motion catalogs (Gaia Collaboration et al. 2018), which allowed us to identify additional member candidates, leading up to a second round of spectroscopic observations with the high resolution Hectochelle instrument on the MMT. We determined the general proper motion of the stream by examining the proper motions of the members selected purely on previously determined radial velocities, specifically those with $260 < V < 318 \text{ km s}^{-1}$. As OphStr extends over several degrees in RA (and galactic longitude), there may be a gradient in proper motions (as reported in Sesar et al. 2015). We first looked at the mean values for the apparently densest part, between $\text{RA}=241$ and 243° . We included proper motion data only where the errors were less than 1.8 mas yr^{-1} for μ_α and less than 1.04 mas yr^{-1} for μ_δ , both of which excluded the worst 10% of the data. These restrictions left us with 45 stars whose radial velocities indicated membership. Fig 5 shows this distribution. As expected, the members have a small range in proper motion, while the field stars have a large dispersion, though the mean values are similar for both groups.

Sesar et al. (2015) measured proper motions of 14 stars determined from astrometry in the USNO-B, 2MASS and PS1 catalogs. These agree in general with the GDR2 values (once transformed to the galactic values that Sesar et al. 2015, published) with the exception of one star (star “rgb4”) for which the measured values are very different from the other radial velocity members in his list, likely due to stated problems with blending. The GDR2 values for that star are similar to the other velocity members, thus this star is considered a member here. For all the stars in common, there is a systematic difference of $+1.0 \text{ mas yr}^{-1}$ in both μ_l and μ_b , with an RMS of the differences of 1 mas yr^{-1} , once we exclude the one bad star. Lane et al. (2019) also found the systematic error in the Sesar et al. (2015) proper motions. Our analysis of the proper motions in galactic

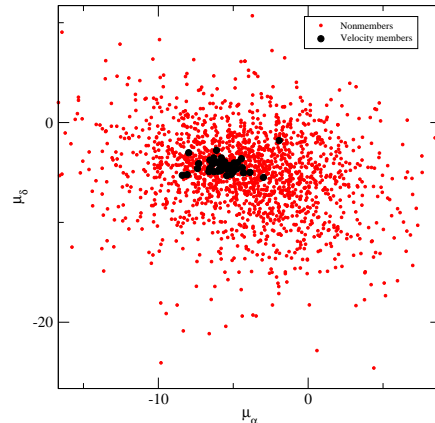


Figure 5. The distribution of Gaia DR2 proper motions for OphStr stars observed spectroscopically with Hectospec, with RA between 241 and 243° , the densest part of the stream. Those stars with radial velocities $260 < V < 318 \text{ km s}^{-1}$ are shown in dark, larger symbols here. The mean proper motion is clearly identified in this plot. Radial velocity member stars with errant proper motions are excluded in the more exacting membership determination provided by the EM method.

coordinates shows agreement with the Lane et al. (2019) description of the proper motions.

Next we derived the relation of μ_α and μ_δ with RA (galactic longitude would work as well). This is shown in Fig. 6 (all of the large points, no matter the color). We then selected stars as candidates for membership by insisting that the stars in the general area of the known stream have Gaia proper motions contained within the distribution shown in the figure, and which also lie in the main sequence area of the CMD as above (Fig 1). A catalog was thus created, and used in the Hectochelle observations that we next describe.

5. 2019 HECTOHELLE DATA

In the latter stages of composing this paper, some additional MMT telescope time became available which was used again with the Hectochelle instrument (Szentgyorgyi et al. 2011), in order to obtain high resolution data for abundance analysis. That work will be reported elsewhere, but we can discuss additional members found in that data for this paper. The observing program consisted mainly of stars in the denser part of

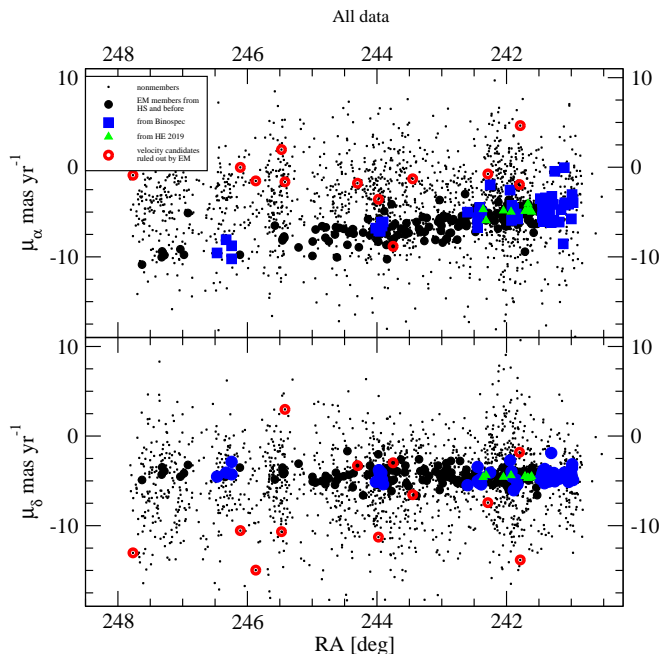


Figure 6. The relation of proper motion in both coordinates with RA for OphStr stars observed spectroscopically with the various instruments reported here. Those stars with radial velocities $260 < V < 318 \text{ km s}^{-1}$ are shown in larger symbols here, in several colors. Small symbols are spectroscopic observations of non-member stars. The EM technique used these clear relations along with the radial velocities to classify the outlier stars (shown in red) as non-members. Large black symbols are members identified using Hectospec and earlier data, while blue represents members found in Binospec data, and green was used for Hectochelle members. The patchiness in this diagram is due to the discrete nature of the observations (we used fields that do not always overlap).

the stream already known to be members, but we also added some previously unobserved stars that satisfied the CMD and proper motion criteria described above, with a preference for stars on the giant branch rather than the MSTO because of the higher spectral resolution being observed. The observing setup was similar to that for the Sesar et al. (2015) data except that a different wavelength region was used : 6135 to 6320 Å. The total exposure time on the single 1° field was 15,700s.

80 stars were targeted (these are also shown in Fig 1, 34 of which provided good velocities. Fortuitously, 9 more members were found in this data, including the brightest member currently known, with $i = 14.8$, which is on the RGB at the brightness level of the HB. All of these members have radial velocities much more precise than the Hectospec, Binospec, or Deimos data, with the mean velocity uncertainty being 0.8 km s^{-1} .

6. USING THE EM TECHNIQUE TO DETERMINE MEMBERSHIP

In summary, we have used three different instruments on the MMT telescope to obtain new spectra and thus radial velocities for targeted stars over a 6° RA extent in the OphStr region. Successful low resolution spectra with uncertainties of order 15 km s^{-1} were obtained for 900 stars using Hectospec and 400 stars using Binospec. Higher resolution Hectochelle data were successfully obtained for 34 more stars, which have uncertainties of order 0.8 km s^{-1} . These radial velocities can of course be used to determine membership, but we can also add in GDR2 proper motions.

The relation between proper motion and RA for radial velocity member stars shown in Fig 6 were used to determine membership, along with positions and radial velocities. These relations were thus incorporated into the statistic used by our “expectation maximization” (EM) code, patterned on that of Walker et al. (2009). EM is an iterative algorithm for estimating the mean and variance of a distribution sampled with contamination. The EM method differs from a conventional, sigma-clipping method in two key respects. First, whereas the conventional method answers the question of membership with a yes or no, the EM method yields estimates of model parameters while evaluating membership of individual stars probabilistically. No data points are discarded; rather, likely contaminants receive appropriately small weights. Second, in evaluating membership probability, the EM method explicitly considers the distributions of both members and contaminants, field stars in this case. Thus, likely contaminants that happen to lie near the center of the member distribution can be identified as such and weighted accordingly. EM therefore allows a full likelihood treatment of the entire data set.

EM can take various observables and select groups from those. It was our task then to determine which observables to use. Aside of the radial velocities, we had available the positions, proper motions, parallaxes and spectral line indices for the Hectospec data. We show below that the parallaxes are at the edge of significance, and thus they did not add any value to membership determination. Likewise, the spectra are fairly low S/N,

and while the spectrum formed by averaging the spectra of members determined with radial velocities and proper motions is clearly different from that of field stars (the stream members have stronger $H\beta$ and weaker Mgb lines, in concordance with a metal-poor population), individual spectra are not good enough to use for spectral analysis, and hence do not contribute significantly to membership determination. Thus we employed only the radial velocities, the proper motions, and the distance from a curved line on the sky (which would be the mean stream position) in the membership search. The location of the stars in the color-magnitude diagram already entered into the selection for spectroscopic observation and would not add any further information in the analysis, and so was excluded. For position, we used the departure from a quadratic equation in the coordinates, rather than distance from a single point as would be the case for a star cluster or dwarf galaxy. In doing so, we explicitly lower the probability of membership for stars that are farther away from this curve, meant to represent the densest part of the stream. For proper motion, we allowed the mean proper motions to have a dependence on coordinates, as discussed in Section 4. In total, we solve for 24 parameters. For members and non-members, we seek a mean radial velocity, mean proper motions, the spread or scale of those values, and their gradients with the two coordinates. Following the description of the method in Walker et al. (2009), we initialize the probabilities at 0.5 for all stars, and solve the equations for the parameter estimates which are similar to Eq. 13 and 14 of Walker et al. (2009). New probability estimates are then calculated, and the procedure is repeated until stability is reached. We typically iterated for 500 steps. In this analysis, there are five stars whose radial velocity would indicate membership, but whose GDR2 data indicate they are not members, not surprising given the distribution of the field stars shown in Fig. 3. Similarly, there are four other stars whose radial velocity would indicate membership (though the errors are large), but which have no data in the GDR2, hence they are also not considered members here.

To estimate the uncertainty of the derived parameters, we further performed a Monte Carlo experiment drawing 1000 samples from the input data set, and running the EM calculation again. The samples were created by creating new samples from the full catalog, with replacement, and using the star’s formal uncertainties in radial velocity and proper motion. The standard deviations of the results for the 24 parameters from the 1000 runs were then calculated. The uncertainty for the velocity dispersion from this heterogeneous data set is not trust-

worthy, nor is the stream dispersion itself, as we discuss below.

Table 3 contains the output of the EM technique, while Table 2 contains a column listing the membership probabilities where all the necessary data exist (position, radial velocity, proper motions and their uncertainties). The members and nonmembers are shown in separate groups in Table 3, with the mean, scale or dispersion, and gradients in ξ (RA coordinate) and η (Dec coordinate) listed. The main distinguishing features between the member group and nonmember group have been shown in various figures already, the large mean radial velocity, the small dispersion in radial velocity and proper motion, and the dependence of proper motion on coordinates. There are currently 203 stars in our study with membership probability $P_{\text{mem}} > 0.9$, and another 15 with a lower threshold of 0.5.

The previous work of Sesar et al. (2015) and Sesar et al. (2016) had identified 14 and 4 possible members, respectively. We confirm all of these as members except for “cand26” from Sesar et al. (2016), which is excluded because its proper motion is out of variance with the other members, in addition to its radial velocity as noted in Sesar et al. (2016).

Fig. 7 shows the distribution of observations on the sky. Light gray circles are those observations for which we could not obtain useful radial velocities, due to low signal-to-noise. Dark circles are used for the successful observations, while red circles shows the members with $P_{\text{mem}} > 0.9$ found using the EM technique (90% of those stars have probabilities greater than 0.95).

We find the following general results. The stream extends over the entire region we observed spectroscopically, from RA=241 to 247° (or $l = 3.8$ to 8° and $b = 27$ to 32.2°). While there is a tight stream as seen before, there are also some high probability stream members significantly away from the main stream. There is no significant detection of a radial velocity gradient (thus perhaps requiring better data to see such a thing). Finally, there is a significant gradient in the RA component of the proper motion with RA itself, as we noted in Fig. 6. The stars away from the tight stream appear to have the same spectral characteristics as those in the main stream (and different from the non-member stars), though higher signal-to-noise spectra would be needed for quantitative analysis.

One of the fields observed with Binospec was a control field, approximately 2° south of the densest part of the stream. Only one star in that field has $P_{\text{mem}} = 0.5$ (and thus not shown in 7, and is thus likely not a member of the OphStr. Thus the stream does not extend to the very large angle of 2° .

Table 3. EM Output

Parameter	Mean	Disp.	Grad ξ^a	Grad η^b	Mean	Disp.	Grad ξ^a	Grad η^b
Members				Nonmembers				
	km s^{-1}	km s^{-1}	km s^{-1}	km s^{-1}	km s^{-1}	km s^{-1}	km s^{-1}	km s^{-1}
			arcmin^{-1}	arcmin^{-1}			arcmin^{-1}	arcmin^{-1}
Velocity	284.4	22.3	-0.019	0.16	-26.4	121.4	-0.067	-0.166
error	2.0	2.5	0.021	0.15	3.02	3.86	0.025	0.093
	mas yr^{-1}	mas yr^{-1}	mas yr^{-1}	mas yr^{-1}	mas yr^{-1}	mas yr^{-1}	mas yr^{-1}	mas yr^{-1}
			arcmin^{-1}	arcmin^{-1}			arcmin^{-1}	arcmin^{-1}
μ_α	-6.63	0.99	-0.015	-0.015	-4.02	4.63	-0.0010	-0.010
error	0.11	0.09	0.001	0.009	0.12	0.09	0.0010	0.004
μ_δ	-4.37	0.73	0.0010	0.001	-5.16	4.46	-0.0040	-0.004
error	0.06	0.07	0.0007	0.007	0.10	0.08	0.0009	0.003

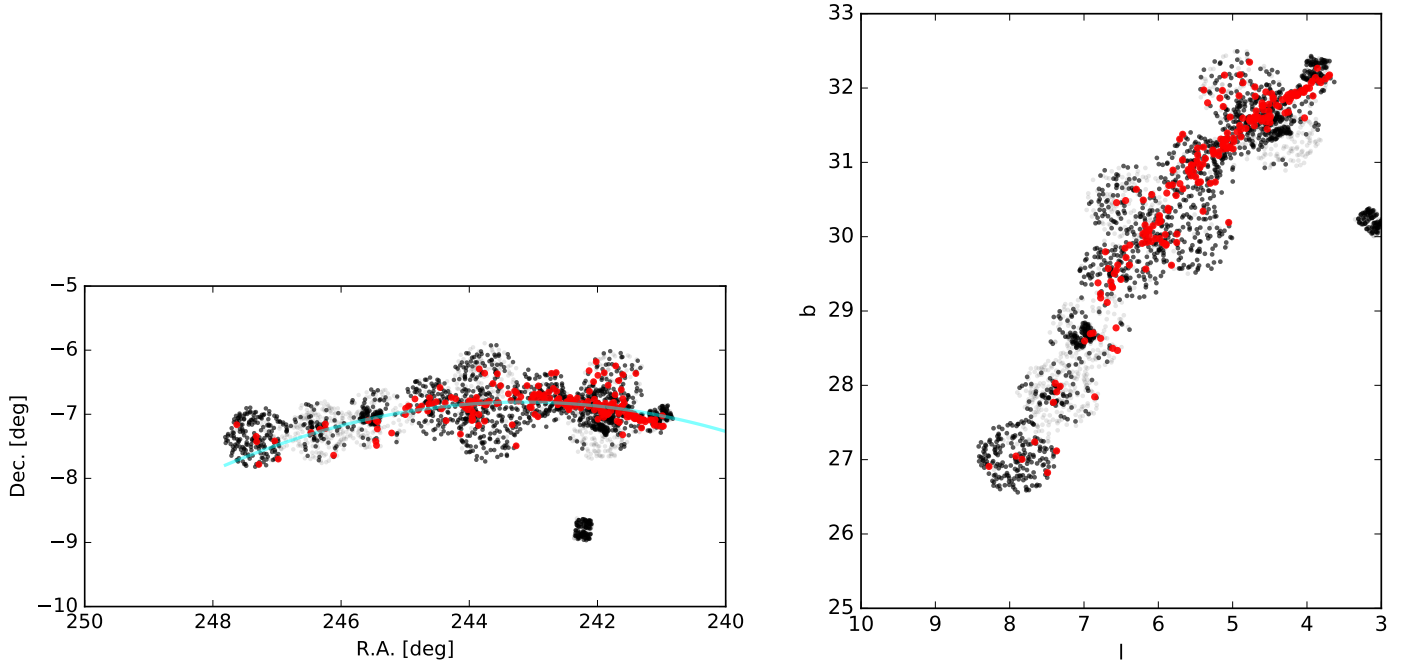
^a Gradient in the RA coordinate^b Gradient in the Dec. coordinate

Figure 7. *Left:* Position on the sky of all spectroscopic observations. The light grey circles are observations that did not result in accurate radial velocities, due to signal-to-noise problems. Dark circles are successful observations. Red circles show the members found by the EM technique (where $P_{\text{mem}} > 0.9$), using radial velocities and proper motions. The solid line is the calculated mean distribution in the form of a quadratic equation, for use in EM (it is not meant to represent a possible orbit). Note the areas where coverage with good observations was poor, but also note the scatter away from the mean distribution for members. *Right:* Same, in galactic coordinates. We omit the line.

Fig. 6 shows the proper motion relations when we use EM membership criteria for the Hectospec and previous data (black points only). The outliers are removed. This then allowed us to determine where best to place new observational fields, with the smaller field of Binospec (and later with more Hectochele observations). Fig 6 also shows the relation when we use EM membership criteria, now including the Binospec data (the blue points).

The velocity dispersion derived for the stream with this heterogeneous data set is $22 \pm 2.5 \text{ km s}^{-1}$. However, the use of low precision data in determining small velocity dispersions is known to result in systematically higher dispersions than true (Koposov et al. 2011). To avoid this issue, we rederived the velocity dispersion using only the Hectochele data for 18 members, which is homogeneous and for which each star has a velocity uncertainly of $< 2.6 \text{ km s}^{-1}$. Our derived velocity dispersion using those stars, which are in the densest part of the stream and in the area from $4.2 < l < 5.0^\circ$ is $1.6 \pm 0.3 \text{ km s}^{-1}$. In Table 2, these are the stars that have $P_{\text{mem}} > 0.9$ and which have either ‘‘F’’ or ‘‘E’’ in the first column. This value is larger than reported in Sesar et al. (2015), even though we reuse 9 of the stars in that paper, along with our 9 new members with similarly precise radial velocities. Indeed, the reported Sesar et al. (2015) value of $0.4^{+0.5}_{-0.4} \text{ km s}^{-1}$ was in fact undetermined.

For orbit analysis, we now have stellar membership probabilities, and can use those values to refine an estimate of the cluster’s length and orbit, which we take up in Section 8.

6.1. A Gaia parallax?

We then explored what the GDR2 parallax catalog could tell us about the distance. Leung & Bovy (2019) and Schönrich et al. (2019) have suggested that the Gaia parallaxes should have $+0.05 \text{ mas}$ added to GDR2 tabulated values, which we will incorporate.

Recall that from modelling the photometric data for 14 member stars, Sesar et al. (2015) had derived a distance modulus of 14.58 and a gradient in the modulus as well, such that the stream at $l = 4$ (perhaps the leading edge of the stream) has a distance of 9 kpc, while 2° away at $l = 6$, the distance was derived to be 7.5 kpc. This was confirmed from the CMD of the new member stars in Section 2.3.2. From our final members list, we downselected to include stars where the formal parallax errors were less than 0.5 mas and which had membership probabilities greater than 0.9. This leaves us with 118 stars spread over 4° in longitude (i.e., twice as long as Sesar et al. 2015). The weighted mean GDR2 parallax of this list is $0.12 \pm 0.01 \text{ mas}$, giving a distance of 8.3

kpc, while that of the 1308 non-members is 0.44 ± 0.004 (2.2 kpc; there are a number of bright stars in this group that are nearby).

What about the distance gradient along the stream? We can form an average parallax for stars grouped at $l = 4$ and 6° as Sesar et al. (2015) considered. The 4° group has 22 stars, with a weighted mean parallax of 0.15, and mean error of 0.07. while the 6° group with 29 stars has a parallax of 0.12 and error of 0.07. Thus, neither is significant though the gradient is in the same sense as the photometry indicates. For the more extended stars found here, at $l > 7^\circ$, we have only 7 stars, whose weighted mean parallax is 0.08, and error of 0.05. The distance change again agrees with the photometry, though the significance is small.

The two brightest member stars (with $i < 15.3$), one RGB star and one BHB star, are located in the dense part of the stream, and $3^\circ 4'$ to the east in the low density area, respectively. These two stars individually have significant detections of parallaxes (at 3.5 and 3.0σ respectively). The average of these is $0.20 \pm 0.03 \text{ mas}$ for a distance of 5.0 kpc (the two stars have similar parallaxes). It appears that the mean GDR2 parallax of radial velocity members is in agreement with the distance from the CMD, but does not add any significance to the measurement.

7. A NEW MAP USING ONLY GAIA AND PS1 DATA

Fig 8 is a simple version of the CMD, with the all input samples shown with the same color, and the members as calculated from Section 6 shown in black. This figure demonstrates that the input sample did not bias the selection of members in the CMD plane, and that the PARSEC isochrone selected in Sesar et al. (2015), along with the distance modulus and gradient is still valid for the members.

Fig 7 highlights two parameters of the stream. First the stream is longer than initially realized in the Bernard et al. (2014) paper. It extends more than $6^\circ 5'$ in RA rather than $2^\circ 5'$. Second, for the western part, there is a tight stream, which is what Bernard et al. (2014) found, but there are also members scattered about that tight area in a more diffuse halo. The extended eastern part of the stream is also diffuse. Because the observing conditions for the observations varied so much, and the fields were not all contiguous, it was not possible to make a satisfactory diagram of the 2D distribution using just the member stars as derived in Section 6. For instance, does the sprinkling of member stars to the north of the dense stream at RA = 242° ($l = 5^\circ$) have a symmetrical distribution to the south? The radial velocity data is not

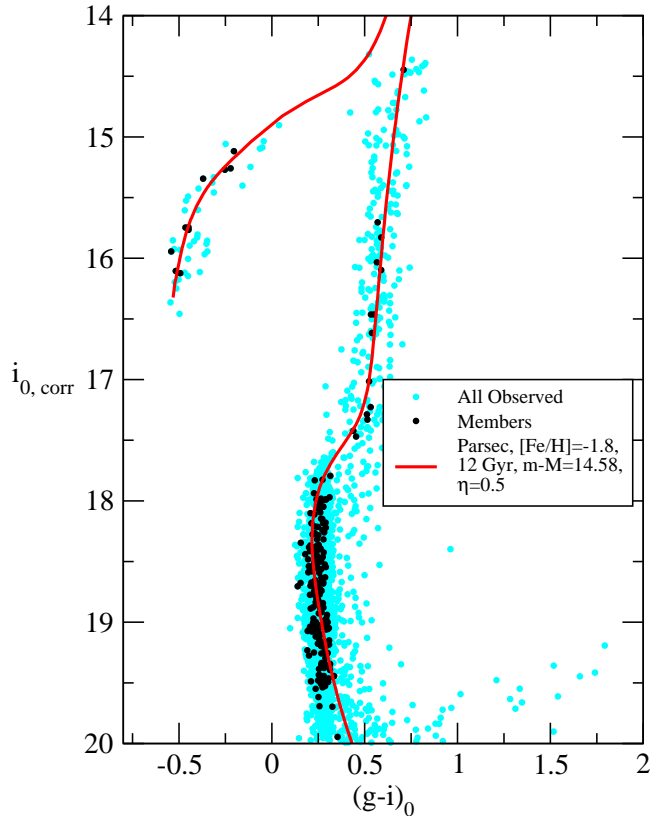


Figure 8. CMD of all stars observed from all data sets including the Binospec data (which are not in Fig. 1), shown as cyan points. Stars with a high probability being members are shown in black. Photometry and isochrone information is the same as for Fig 1.

complete enough to answer that. We can alleviate the problems produced by the spatial incompleteness of the radial velocity data by making a revised map using the positions and photometry of likely members from a stellar catalog such as PS1 combined with proper motions from GDR2. While the stream’s proper motions do not readily distinguish it from the other stars in the field (see Fig 5) as well as the radial velocity measurements do, the mean motion does provide an additional selection criterion. We used the refined CMD locus from the known members and the GDR2 catalog and were able to produce an image that does better reflect the large-scale distribution of stars than revealed in the radial velocity measurements.

In detail, we assigned membership probabilities from the PS1 and GDR2 catalogs. For the CMD filtering, the

best fitting isochrone remains the one from PARSEC, with $[\text{Fe}/\text{H}] = -1.8$, $\text{age} = 12 \text{ Gyr}$, $\eta = 0.5$, $m - M = 14.58$, and with the Sesar et al. (2015) distance modulus gradient, $m - M = 14.58 - 0.2(l - 5)$. For a star with color and magnitude, $(g - i)_0$ and $i_{0, \text{corr}}$, the difference between the observed color and that of the isochrone at the star’s i -band magnitude was calculated, and turned into a probability via $\text{abs}((g - i)_0 - (g - i)_{\text{isochrone}}) / \sigma_{\text{rel}}$, where σ_{rel} is the spread in the observed catalog about the isochrone, at magnitude $i_{0, \text{corr}}$. We used stars in the region of the HB, the main sequence brighter than $i_{0, \text{corr}} = 20.0$ ($i = 20.4$), and the giant branch up to about 1 magnitude below the level of the HB, which was about $i_{0, \text{corr}} = 15.5$ (or observed $i = 15.8$). Proper motions were used in a similar fashion, this time using the distance to the mean relation of proper motion with coordinates as defined by the radial velocity members (Fig. 6) divided by the spread in that relation. These quantities were summed quadratically along with the CMD probability for each star, and turned into a transparency value for graphical purposes. Fig. 9 shows the result, in galactic coordinates. The CMD filtering alone provides most of the contrast in this diagram, but the addition of the proper motion filtering eliminates much of the remnant dust dependency of the CMD filter. Adding in the giant stars to the MS and BHB list did not add much contrast to this figure; only ten percent of the stars shown are giant candidates. Removing stars with accurate parallaxes indicating non-membership also did not achieve much; there were only 50 such stars. In total, there are about 2400 stars remaining after the selection criteria were applied.

Fig. 9 confirms the map made using the additional parameter of the radial velocities: a nearly-linear, tight stream extending from $l = 3^{\circ}2$ to $5^{\circ}8$ (380 pc), and a longer more diffuse tail with more curvature (in these projected coordinates) extending as far as $l = 8^{\circ}$ for a total length of 7.5° , or 1.1 kpc in projection. The leading edge of the stream in the radial velocity membership is $l = 3^{\circ}8$, but the proper-motion/CMD map alone shows the distinct edge to actually be at $\text{RA} = 239.8$, $\text{DEC} = -7.24$ ($l = 3^{\circ}2$, $b = 32^{\circ}4$), which is $0^{\circ}5$ farther from the edge of the spectroscopic coverage. If the leading edge also has a diffuse component, it is possible that the stream extends beyond our catalog’s footprint, but we leave mapping the full extent of the stream to future work. Using the same distance modulus gradient as found in Sesar et al. (2015), the deprojected length of the currently-detected stream is about 3 kpc.

Finally, Fig. 9 confirms the presence, noticed in the radial velocity work, of members in a curious arc-like structure that arches in latitude away from the main

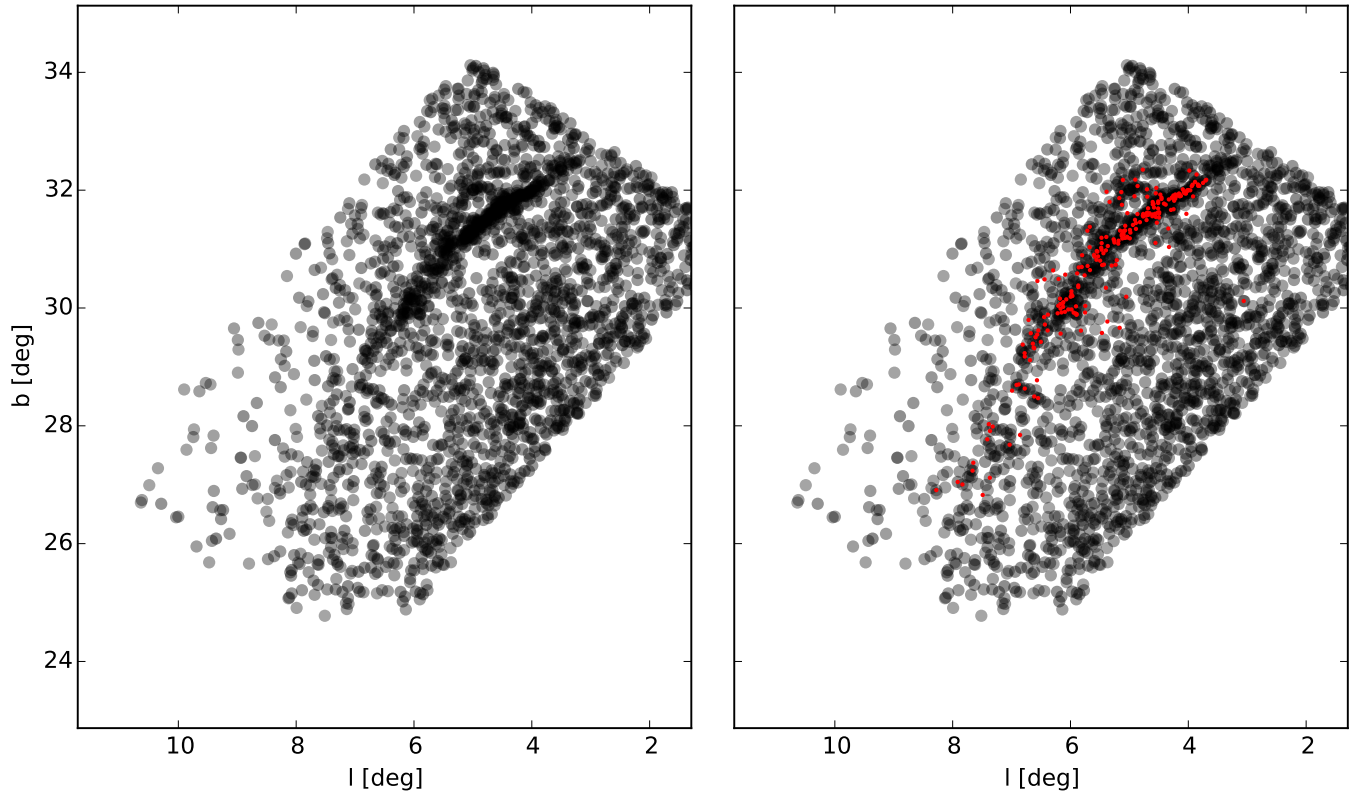


Figure 9. Using the measured proper motion and distance modulus gradient for the stream, we selected HB, MSTO and lower RGB stars from the full GDR2 catalog for display. Probabilities of stream membership were based on deviation from the isochrone used above, and also from the relation of proper motion and position determined above. No radial velocities were used. On the right the stars observed spectroscopically and which have stream membership probabilities of greater than 50% are shown in red, revealing there to be good correspondence, even for stars away from the main stream.

stream at $l = 4$, to a separation of nearly a degree, and then apparently rejoins the main stream at $l = 6$. Recall that for the EM analysis above, stars farther from the main stream are explicitly judged to have lower membership probabilities, so the number of EM member stars in this spur may be an underestimate. A topic for future investigation would be whether this sub-stream is similar to the spurs on GD-1 and Jhelum found and discussed in Price-Whelan, & Bonaca (2018), Bonaca et al. (2019a) and Bonaca et al. (2019b).

8. ORBIT FITTING

In this section we revise the orbital properties of Oph-Str given the newly detected extension of the stream. Figure 10 summarizes the 6D phase-space distribution of likely Ophiuchus members. From top to bottom, we show Dec, distance, RA and Dec components of the proper motion vector, and radial velocity as a function of RA, with the errorbars representing the observational uncertainties. The proper motion uncertainties are delivered by GDR2, while we adopted the stream width of 0.3° as the uncertainty in sky positions, and assumed

0.5 kpc uncertainty in distances, and 10 km s^{-1} for radial velocities. We use these data to search for plausible orbits of the OphStr progenitor.

In our modeling, we used a static Milky Way potential that has a $5.5 \times 10^{10} M_\odot$ Miyamoto & Nagai (1975) disk (scale height 28 pc, scale length 3 kpc), a $4 \times 10^9 M_\odot$ Hernquist (1990) bulge (scale radius 1 kpc), and a $7 \times 10^{11} M_\odot$ Navarro et al. (1997) halo (scale radius 15.62 kpc, z -axis flattening 0.95), as implemented in the *gala* package (Price-Whelan 2017). To convert between the physical and observed (heliocentric) quantities, we adopted a right-handed coordinate system with the origin at the Galactic center in which the Sun is located at $(X, Y, Z) = (-8.122, 0, 0.0208)$ kpc and is moving at velocity $(V_X, V_Y, V_Z) = (12.9, 245.6, 7.78) \text{ km s}^{-1}$ (available in *astropy* version 4.0). We searched for a best-fitting orbit in this gravitational potential by minimizing the deviations between the orbit and individual stars using the *scipy* implementation of the BFGS algorithm. We evaluated trial orbits at RA positions of likely Ophiuchus members, taking into account the ob-

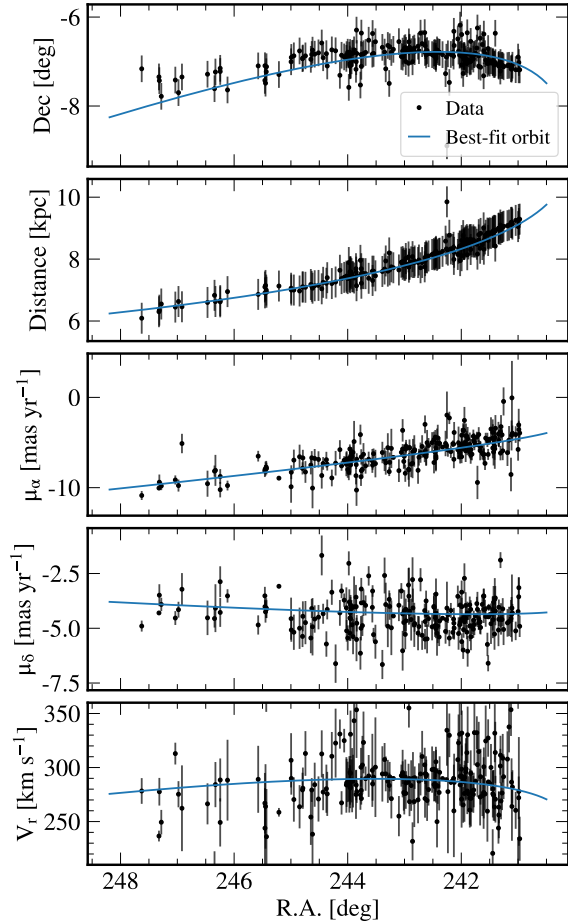


Figure 10. Phase-space distribution of likely Ophiuchus member stars (black points) and the best-fit orbit in a smooth and static Milky Way potential (blue lines).

servational uncertainties. The best-fit orbit is shown with blue lines in Figure 10.

The orbit which was evolved in a simple, static Milky Way potential captures the global phase-space distribution of the OphStr stream, including the newly discovered extension at $RA \gtrsim 244^\circ$. The best-fit orbit reproduces well the observed gradients in distance, proper motions and radial velocity. This orbit is somewhat misaligned from the observed stream track, as expected of streams in general (e.g., Sanders & Binney 2013).

The past 3 Gyr of Ophiuchus’ orbit are shown in Figure 11 in light blue, while the current extent of the stream is emphasized in dark blue. The stream is just past the pericenter, which occurred at ≈ 3.8 kpc, in agreement with previous orbit determinations using the densest part of the stream (Sesar et al. 2015; Lane et al. 2019). However, we inferred a smaller apocenter of 13.5 kpc than previously derived 16.8 kpc, which directly translates to a shorter period of 172 Myr (com-

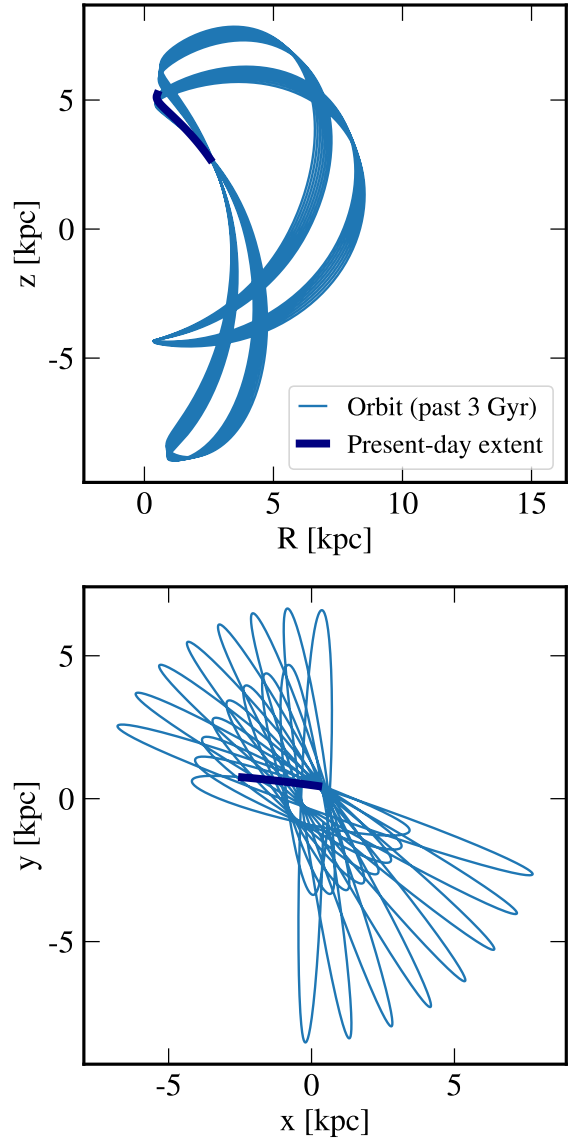


Figure 11. The best-fit orbit to the Ophiuchus stream in the Galactocentric coordinates perpendicular to the disk plane (top), and in the disk plane (bottom). The Sun is at $z=0$, $R=8$ kpc in the top plot. Current extent of the stream is shown in dark blue, while the past 3 Gyr are in light blue.

pared to 240 Myr). Generally, we expect longer streams to be more informative (Bonaca & Hogg 2018), and therefore our orbit which fits a longer segment of the stream to be more accurate. In addition, this is the first self-consistent orbit fit using the accurate Gaia proper motions, which might contribute to the change in the derived orbit. Fits to the latest Ophiuchus data place its progenitor on a somewhat less eccentric orbit than previously estimated, so dynamical models aiming to reproduce the observed stream should be revised to use this new orbit.

9. DISCUSSION AND CONCLUSIONS

Our spectroscopic work has increased the number of probable members ($P_{\text{mem}} > 0.9$) of the Ophiuchus stream from the 18 reported previously to about 200, which lie along an arc 7.5° long in projection, or about 3 kpc deprojected. In finding these new members and candidates however, we have not significantly increased the estimated luminosity of the progenitor cluster found by Bernard et al. (2014) of $M_V = -3.0$, or the estimated mass of $2 \times 10^4 M_\odot$ from Sesar et al. (2015). Using our new method for finding probable members from the GDR2 and PS1 data (Sect. 7), and a correction provided by the luminosity function for the Parsec isochrone used in Sect. 2 we derived fewer total stars brighter than $i=20$ than Sesar et al. (2015) (thus our calculated surface brightness is lower), resulting in a new calculated luminosity of the entire stream of $M_V = -3.1$, and a total mass of $8700 \pm 400 M_\odot$, where the uncertainty comes from counting statistics only, and is likely an underestimate.

While the new low resolution spectra have allowed us to explore the distribution of members and refine orbit models, few of the derived radial velocities are as precise as one would need for mass estimates. In particular, the low resolution data appears to allow the velocity variation with longitude outlined here as well as those in Price-Whelan et al. (2016, their figure 2) or Lane et al. (2019, their figure 3). To independently constrain the mass of the OphStr progenitor, we only use the high-resolution Hectochelle data and obtain a new velocity dispersion value of $1.6 \pm 0.4 \text{ km s}^{-1}$. Empirically, we expect the velocity dispersion in the cluster to be similar or lower than in its tidal tails (for example, the dispersion in the Palomar 5 globular cluster is 1.2 km s^{-1} and 2.1 km s^{-1} in its tails, Odenkirchen et al. 2009; Kuzma et al. 2015). There are six clusters in the Harris (2010) catalog with velocity dispersions equal to or less than 1.6 km s^{-1} , however, these are all somewhat more luminous than our value for OphStr. However, dynamical heating of tidal tails may resolve this inconsistency between the inferred mass and velocity dispersion. Specifically, Lane et al. (2019) simulated globular clusters with a range of masses and sizes on OphStr orbits, and their more diffuse progenitors of $\approx 8700 M_\odot$ achieve a velocity dispersion of $> 1 \text{ km s}^{-1}$ after three complete orbital periods. Similar simulations that include our new constraints on the OphStr extent and radial velocity dispersion will further refine our initial estimate of its progenitor’s mass.

The stream orbit as refined by this new data is smaller than previously determined, with a period of 172 Myr and an apocenter of 13.5 kpc. This would indicate

that the galactic bar should have an even larger influence on the stream dynamical evolution than previously thought.

Similar to previous papers on OphStr, we did not find a progenitor star cluster for OphStr, unlike the case for the Palomar 5 stream (Price-Whelan et al. 2019). Interestingly, we did find evidence for vertical sub-structure in the form of a spur. Bonaca et al. (2019b) showed that spurs can be produced if a stream encounters a massive object, such as a dark-matter subhalo or a globular cluster. The abundance of dark-matter subhalos is expected to be severely depressed in the inner Galaxy due to disk disruption (e.g., D’Onghia et al. 2010; Er-rani et al. 2017; Garrison-Kimmel et al. 2017), but most Galactic globular clusters orbit in the same volume as OphStr (e.g., Baumgardt et al. 2019). Precise kinematic maps of the affected region in the stream can constrain the impactor’s orbit (Bonaca et al. 2020), motivating additional high-resolution spectroscopy of OphStr to uncover its complex dynamical history.

Software: Astropy (Astropy Collaboration et al. 2013, 2018), gala (Price-Whelan 2017), matplotlib (Hunter 2007), numpy (Walt et al. 2011), scipy (Jones et al. 2001–)

ACKNOWLEDGMENTS

We thank Martin Paegert, Sean Moran, and the MMT remote observers for help in obtaining the telescopic and archival data. We also thank Christian Johnson, Gyuchul Myeong, John Raymond, Joel Pfeffer, and Julio Navarro for illuminating conversations. NSF Grant AST-1812461 supported work on this project.

REFERENCES

- Astropy Collaboration, Robitaille, T. P., Tollerud, E. J., et al. 2013, *A&A*, 558, A33
- Astropy Collaboration, Price-Whelan, A. M., Sipőcz, B. M., et al. 2018, *AJ*, 156, 123
- Balbinot, E., & Gieles, M. 2018, *MNRAS*, 474, 2479
- Baumgardt, H., Hilker, M., Sollima, A., & Bellini, A. 2019, *MNRAS*, 482, 5138
- Bernard, E. J., Ferguson, A. M. N., Schlafly, E. F., et al. 2014, *MNRAS*, 443, L84
- Bonaca, A., & Hogg, D. W. 2018, *ApJ*, 867, 101
- Bonaca, A., Conroy, C., Price-Whelan, A. M., et al. 2019a, *ApJL*, 881, L37
- Bonaca, A., Hogg, D. W., Price-Whelan, A. M., et al. 2019b, *ApJ*, 880, 38
- Bonaca, A., Conroy, C., Hogg, D. W., et al. 2020, *ApJL*, 892, L37
- Bressan, A., Marigo, P., Girardi, L., et al. 2012, *MNRAS*, 427, 127
- Caldwell, N., Harding, P., Morrison, H., et al. 2009, *AJ*, 137, 94
- D’Onghia, E., Springel, V., Hernquist, L., & Keres, D. 2010, *ApJ*, 709, 1138
- Errani, R., Peñarrubia, J., Laporte, C. F. P., & Gómez, F. A. 2017, *MNRAS*, 465, L59
- Fabricant, D., et al. 2005, *PASP*, 117, 1411
- Fabricant, D., Fata, R., Epps, H., et al. 2019, *PASP*, 131, 075004
- Gaia Collaboration, Brown, A. G. A., Vallenari, A., et al. 2018, *A&A*, 616, A1
- Garrison-Kimmel, S., Wetzel, A., Bullock, J. S., et al. 2017, *MNRAS*, 471, 1709
- Grillmair, C. J., & Carlin, J. L. 2016, *Tidal Streams in the Local Group and Beyond*, 87
- Haffner, L. M., Reynolds, R. J., Tufte, S. L., et al. 2003, *ApJS*, 149, 405
- Harris, W. E. 2010, arXiv e-prints, arXiv:1012.3224
- Hattori, K., Erkal, D., & Sanders, J. L. 2016, *MNRAS*, 460, 497
- Hernquist, L. 1990, *ApJ*, 356, 359
- Hunter, J. D. 2007, *Computing in Science and Engineering*, 9, 90
- Jones, E., Oliphant, T., Peterson, P., et al. 2001–, *SciPy: Open source scientific tools for Python*, .
<http://www.scipy.org/>
- Kaiser, N., Burgett, W., Chambers, K., et al. 2010, *Proc. SPIE*, 7733, 77330E
- Koposov, S. E., Gilmore, G., Walker, M. G., et al. 2011, *ApJ*, 736, 146
- Kurtz, M. J., & Mink, D. J. 1998, *PASP*, 110, 934
- Kuzma, P. B., Da Costa, G. S., Keller, S. C., & Maunder, E. 2015, *MNRAS*, 446, 3297
- Lane, J. M. M., Navarro, J. F., Fattahi, A., Oman, K. A., & Bovy, J. 2019, arXiv e-prints, arXiv:1905.12633
- Leung, H. W., & Bovy, J. 2019, arXiv e-prints, arXiv:1902.08634
- Miyamoto, M., & Nagai, R. 1975, *PASJ*, 27, 533
- Navarro, J. F., Frenk, C. S., & White, S. D. M. 1997, *ApJ*, 490, 493
- Odenkirchen, M., Grebel, E. K., Kayser, A., Rix, H.-W., & Dehnen, W. 2009, *AJ*, 137, 3378
- Price-Whelan, A. M., B. Sesar, K. V. Johnston, and H.-W. Rix, 2016, *ApJ*, 824, 104
- Price-Whelan, A. M. 2017, *The Journal of Open Source Software*, 2, 388
- Price-Whelan, A. M., & Bonaca, A. 2018, *ApJL*, 863, L20
- Price-Whelan, A. M., Mateu, C., Iorio, G., et al. 2019, arXiv e-prints, arXiv:1910.00595
- Sanders, J. L., & Binney, J. 2013, *MNRAS*, 433, 1813
- Schlafly, E. F., Green, G., Finkbeiner, D. P., et al. 2014, *ApJ*, 789, 15
- Schlegel, D. J., Finkbeiner, D. P., & Davis, M. 1998, *ApJ*, 500, 525
- Schönrich, R., McMillan, P., & Eyer, L. 2019, *MNRAS*, 487, 3568
- Szentgyorgyi, A., Furesz, G., Cheimets, P., et al. 2011, *PASP*, 123, 1188
- Sesar, B., Bovy, J., Bernard, E. J., et al. 2015, *ApJ*, 809, 59
- Sesar, B., Price-Whelan, A. M., Cohen, J. G. et al. 2016, *ApJL*, 816, 4
- Strader, J., Caldwell, N., & Seth, A. C. 2011, *AJ*, 142, 8
- Walker, Matthew G., Mateo, M. et al. 2009, *AJ*, 137, 3109
- Walt, S. v. d., Colbert, S. C., & Varoquaux, G. 2011, *Computing in Science and Eng.*, 13, 22.
<http://dx.doi.org/10.1109/MCSE.2011.37>